Engineering Structures 159 (2018) 66–74

Contents lists available at ScienceDirect

Engineering Structures

journal homepage: www.elsevier.com/locate/engstruct

Mobile impact testing of a simply-supported steel stringer bridge with reference-free measurement

Shuanglin Guo[a], Xin Zhang[b], Jian Zhang[a,*], Yun Zhou[c], Franklin Moon[d], A. Emin Aktan[e]

[a] Jiangsu Key Laboratory of Engineering Mechanics, Southeast University, Nanjing 210096, China
[b] Hualu Transport Technology Co.,Ltd, Guangzhou 510800, China
[c] College of Civil Engineering, Hunan University, Changsha 410082, China
[d] Department of Civil and Environmental Engineering, Rutgers, The State University of New Jersey, NJ 08854, USA
[e] Department of Civil, Architectural & Environmental Engineering, Drexel University, PA 19104, USA

ARTICLE INFO

Keywords:
Mobile impact test
Scaling factor
Flexibility
Reference nodes
Structural identification

ABSTRACT

Mobile impact testing of a simply-supported steel stringer bridge is investigated for efficient structural flexibility identification. The classical impact test method requires a number of sensors deployed on the entire structure; in contrast, this paper proposes a novel mobile impact test method that sequentially measures segments of the entire structure with much fewer sensors. The advantage of the proposed approach lies in that it greatly reduces the experimental cost, and it can output the same results of the entire structure's flexibility matrix as the traditional impact test method. In the proposed method, the data processing algorithm is developed to integrate the measurements of all segments for identifying the entire structure's flexibility matrix. Especially, it does not need any transitional nodes to be references by adopting the principle of minimum potential energy, which greatly improves the efficiency of mobile impact testing. Application of the proposed approach to a simply-supported steel stringer bridge successfully verifies its feasibility and efficiency.

1. Introduction

Ambient vibration test using traffic flows and wind loads to excite structures are convenient to perform [1–8], which mainly output preliminary modal parameters (natural frequencies, damping and mode shapes). However, it is still difficult to effectively identify the location and quantify the degree of damages in civil structures even though a lots of damage detection methods have been developed by using the modal parameters identified from ambient vibration data [9,10]. This is mainly due to the large spatial extent of civil structures, fair amount of obscure construction details and a large number of structural elements interacting with each other in a way that is currently not fully quantifiable [11]. Another promising way for structural vibration test is the controllable impact test. Brown et al. [12] and Zhou et al. [13] used the sledge hammer to impact the bridge, during which the input force and structural responses are recorded to identify structural scaling factors and the flexibility matrix. The identified flexibility results are useful for structural performance evaluation as shown in Fig. 1. First, it is useful to investigate force-deflection information of the studied bridge. Structural deflections can be predicted by multiplying the static load by the identified flexibility matrix. They are comparable with the measured ones from static track load test which is an important experiment tool for evaluating the load carrying capacity of short/middle-span bridges [13,14]. Second, the identified flexibility can be used to develop structural damage indexes, which has been proved to be more effective for structural damage detection than common frequency or mode shape based damage indexes [15].

The impact test has the merit to identify the scaling factor and the flexibility as described above. It has not been widely applied in engineering practices because it is not as convenient as ambient vibration test to perform. Inspired by the idea of bridge rapid testing developed recently [16–18], researchers have developed onboard impacting devices to improve the efficiency of impact test [15,19]. On the other hand, mobile impact testing which divides the whole structure into substructures for consecutive testing has been developed to further speed up the impact test. Traditional impact test requires a number of sensors deployed on the entire structure (Fig. 1), which induces high hardware cost and experimental time. The strategy of mobile testing perform the impact test of the substructure one by one as shown in Fig. 2, thus the number of required sensors are greatly reduced. However, the arising question is how to integrate the test data of substructure to identify the mode shapes and the flexibility of the entire structure. Zhang et al. [20] first developed a mobile impact testing method as shown in Fig. 2(a), in which the interface nodes of two

* Corresponding author.
E-mail address: jian@seu.edu.cn (J. Zhang).

https://doi.org/10.1016/j.engstruct.2017.12.020
Received 5 March 2017; Received in revised form 9 December 2017; Accepted 12 December 2017
Available online 30 December 2017

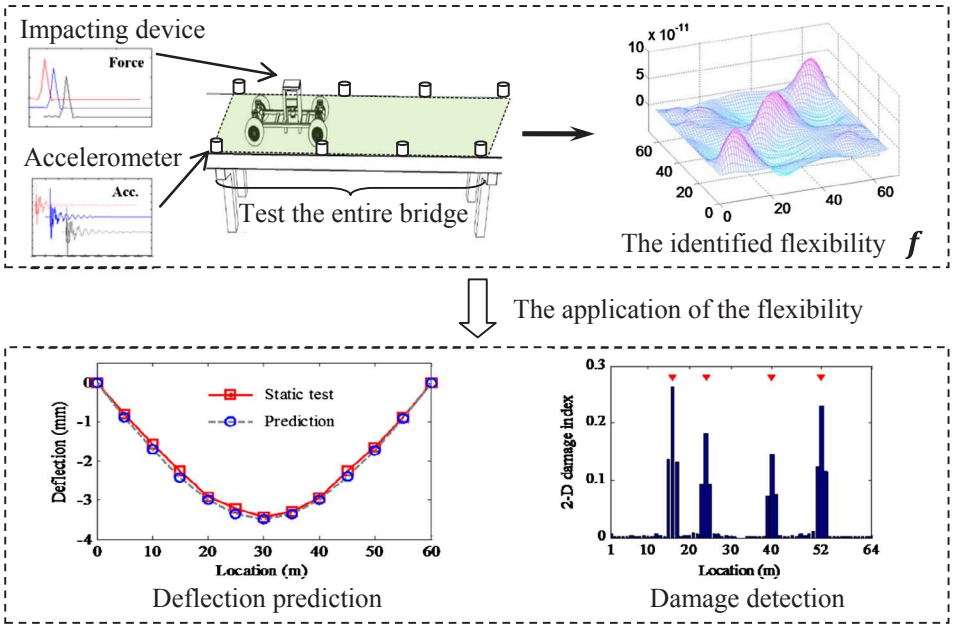

Fig. 1. The purpose to identify structural flexibility matrix.

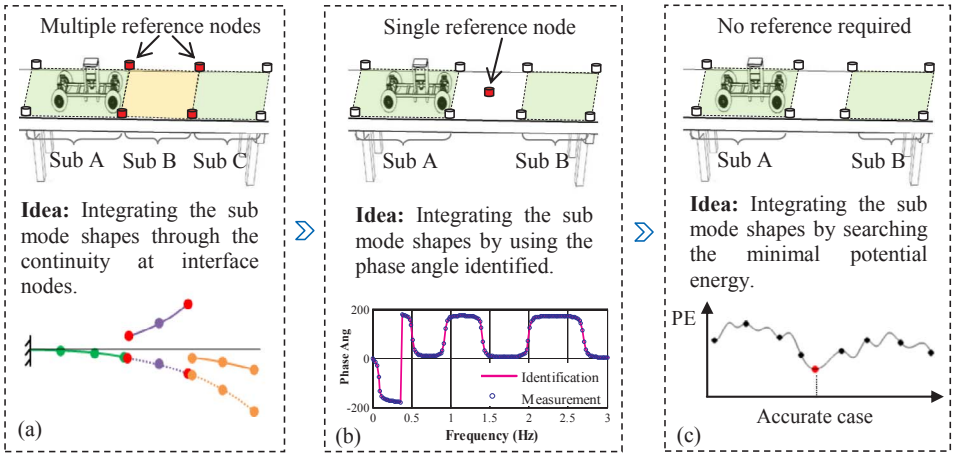

Fig. 2. Development of the mobile impact test methods: (a) multiple-reference; (b) single-reference; (c) reference-free.

adjacent substructures are required to be taken as reference nodes in order to integrate the mobile test data. It should be noted that the efficiency of the mobile test will be decreased with the increasing number of reference nodes, because the responses of those reference nodes are required to be repetitively measured during the impact tests of all substructures. To further speed up the mobile impact test, Zhang et al. [21] developed a mobile impact test method as shown in Fig. 2(b), which only requires a single reference node. In this article, the mobile impact test without requiring the reference node as shown in Fig. 2(c) will be proposed, in which a new idea of searching the minimum potential energy (PE) of the structure is proposed to integrate the test data of substructures. Evidently the reference-free strategy is the most efficient way for engineering application.

2. Methodology of the reference-free mobile impact test

2.1. Basic idea

By taking a seven degree-of-freedom (DOF) beam model (Fig. 3) as the example for illustration of the mobile impact test, the structure is independently divided into three substructures which will be tested one by one in the proposed method. Because there are no reference nodes required in the proposed test scheme, it greatly increase the test speed, but the challenging problem arising is that how the substructures' data are integrated for identification of the entire structure.

For the Sub A in Fig. 3, the FRF $\boldsymbol{H}^{\mathbf{AA}}(\omega) \in \mathbb{C}^{N_o^A \times N_i^A}$ are estimated from the impact test data, where the symbol "$\mathbb{C}$" denotes the sets of complex numbers, and N_o^A and N_i^A are the number of output and input nodes of Sub A respectively. Directly integrating the estimated FRFs of Sub A, Sub B and Sub C leads to a sparse FRF matrix of the entire structure $\boldsymbol{H}^{\boldsymbol{ABC}}(\omega)$ and correspondingly the sparse structural flexibility matrix can be identified, i.e., all elements locating on the non-diagonal regions of the matrix still unknown. The proposed data processing strategy aims to identify the full matrix of the entire structure $\boldsymbol{f}^{\boldsymbol{ABC}}$ as illustrated in Fig. 3, in which $\boldsymbol{f}^{\boldsymbol{AA}} \in \mathbb{R}^{N_o^A \times N_o^A}$ is the flexibility matrix of Sub A and the symbol "$\mathbb{R}$" denotes the sets of real numbers.

2.2. Difficulty to assemble substructure mode shapes

Modal parameters of three substructures in Fig. 3 are identified. The identified r-th frequency ω_r, damping ratio ξ_r and system pole $\lambda_r = -\xi_r\omega_r + j\omega_r\sqrt{1-\xi_r^2}$ of the three substructures are close. Other identified modal parameters include modal scaling factors, mode shapes and modal participation factors, which are denoted by $\{Q_r^A, \boldsymbol{\phi}_r^A, \boldsymbol{L}_r^A\}$, $\{Q_r^B, \boldsymbol{\phi}_r^B, \boldsymbol{L}_r^B\}$ and $\{Q_r^C, \boldsymbol{\phi}_r^C, \boldsymbol{L}_r^C\}$ for the three substructures respectively. It is worth noting that the estimated mode shapes of the three substructures do not have the same scaling level because they are

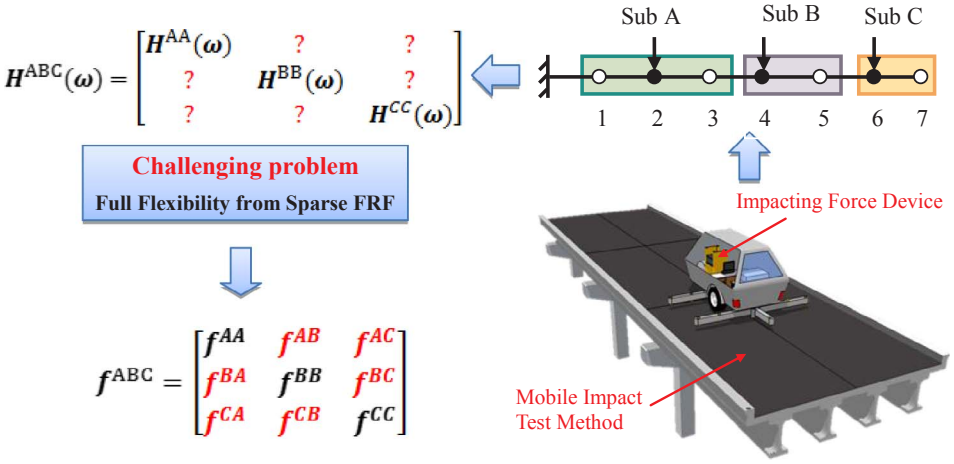

Fig. 3. Mobile impact testing with reference-free measurement.

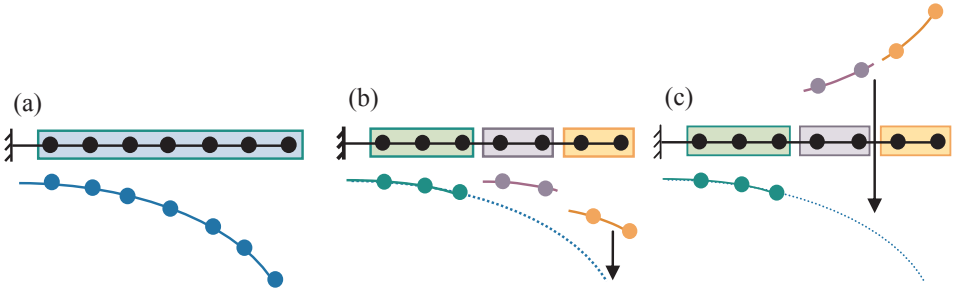

Fig. 4. Mode shapes integration: (a) The structure mode shape; (b) Magnitude scaling; (c) Sign adjustment.

tested independently. That is to say, their modal scaling factors are different, $Q_r^A \neq Q_r^B \neq Q_r^C$, thus the three substructures' mode shapes cannot be concatenated directly to produce the global mode shape of the entire structure (Fig. 4(a)) for full flexibility matrix identification. Thus the work adjusting the magnitudes (Fig. 4(b)) and the signs (Fig. 4(c)) of substructures' mode shapes to be consistent has to be performed.

3. Theory development

3.1. Magnitude scaling

Sub A is taken as the master substructure. Correspondingly, Sub B and Sub C are the subordinate substructures. In order to revise the mode shape of Sub B such that they have the same modal scaling factor (i.e. $\widetilde{Q}_r^B = Q_r^A$), an adjusting factor α_r^B is used to adjust the mode shape $\boldsymbol{\phi}_r^B$ to be $\widetilde{\boldsymbol{\phi}}_r^B = \alpha_r^B \boldsymbol{\phi}_r^B$, and an another adjusting factor β_r^B is employed to adjust the modal participation factor $\boldsymbol{L}_r^B$ to be $\widetilde{\boldsymbol{L}}_r^B = \beta_r^B \boldsymbol{L}_r^B$. Note that the adjusting factors α_r^B and β_r^B are real values.

The magnitudes of the two unknown adjusting factors α_r^B and β_r^B can be solved by using identified modal parameters. The detailed derivation process please refers to [21]. However, their signs are still unknown, which means that the orientations of substructures' mode shapes are still undetermined as illustrated in Fig. 4(c). Tentatively defining η_r^B as the undetermined sign factor (i.e., $\eta_r^B = 1$ or -1) of the r-th mode, α_r^B and β_r^B can be rewritten as follows.

$$\alpha_r^B = \eta_r^B \sqrt{\frac{Q_r^B}{Q_r^A}}, \quad \beta_r^B = \eta_r^B \sqrt{\frac{Q_r^A}{Q_r^B}} \tag{1}$$

According to the rotation rule, the adjusting factor, α_r^C and β_r^C, of the r-th mode of Sub C can be obtained easily. The process of scaling the mode shapes of subordinate substructures is illustrated in Step 3 of Fig. 5. The global mode shape $\boldsymbol{\phi}_r$ and the global modal participation factor $\boldsymbol{L}_r$ after the adjusting operation completes can be obtained as

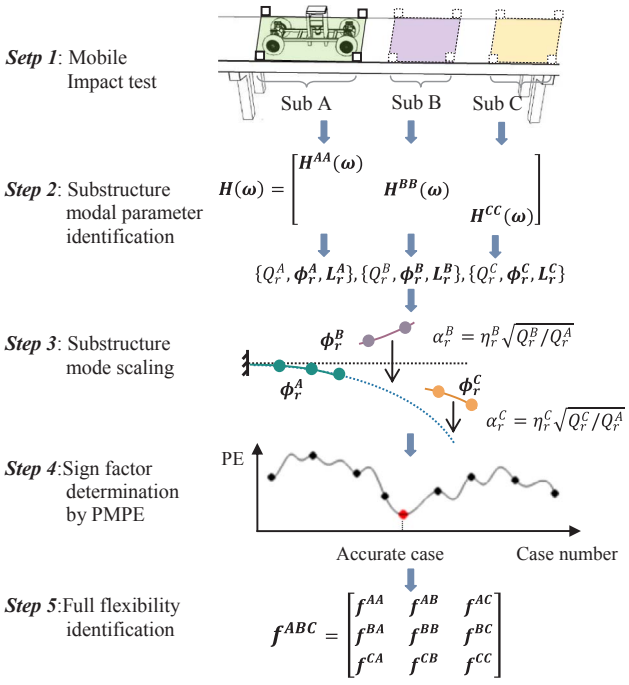

Fig. 5. Overview of the methodology.

follows:

$$\boldsymbol{\phi}_r = \begin{bmatrix} \boldsymbol{\phi}_r^A \\ \eta_r^B \sqrt{\frac{Q_r^B}{Q_r^A}} \boldsymbol{\phi}_r^B \\ \eta_r^C \sqrt{\frac{Q_r^C}{Q_r^A}} \boldsymbol{\phi}_r^C \end{bmatrix}, \quad \boldsymbol{L}_r = \begin{bmatrix} \boldsymbol{L}_r^A \\ \eta_r^B \sqrt{\frac{Q_r^A}{Q_r^B}} \boldsymbol{L}_r^B \\ \eta_r^C \sqrt{\frac{Q_r^A}{Q_r^C}} \boldsymbol{L}_r^C \end{bmatrix} \tag{2}$$

If the sign factors η_r^B and η_r^C in Eq. (2) kwnon, the modal parameters

of the entire structure terming as $\{\lambda_r, Q_r, \boldsymbol{\phi_r}, \boldsymbol{L_r}\}$ can be achieved, among which the system poles and the modal scaling factors of the entire structure utilize λ_r^A and Q_r^A of the master substructure. The flexibility matrix is written as shown below [21]:

$$\boldsymbol{f}(\eta_r^B, \eta_r^C) = \sum_{r=1}^{m} \left(\frac{\boldsymbol{\phi_r}(\boldsymbol{\phi_r})^{\mathrm{T}} Q_r}{-\lambda_r} + \frac{\boldsymbol{\phi_r^*}(\boldsymbol{\phi_r^*})^{\mathrm{T}} Q_r^*}{-\lambda_r^*} \right) \tag{3}$$

where m is the mode number. Namely, the flexibility matrix is represented as a function with respect to η_r^B and η_r^C because they are unknown so far.

3.2. Sign factor determination by utilizing PMPE

For elastic bodies in equilibrium, real deformation occurred minimizes the potential energy of the object, which is the principle of minimum potential energy (PMPE) [22]. The flexibility matrix $\boldsymbol{f}(\eta_r^B, \eta_r^C)$ calculated by Eq. (3) through any combinations of the sign factors η_r^B and η_r^C can be used to predict structural displacement vector $\boldsymbol{u}(\eta_r^B, \eta_r^C)$ under the load vector $\boldsymbol{F}$:

$$\boldsymbol{u}(\eta_r^B, \eta_r^C) = \boldsymbol{f}(\eta_r^B, \eta_r^C)\boldsymbol{F} \tag{4}$$

Because different combinations of sign factors lead to different displacement predictions, the potential energies of the structure calculated by those predicted displacements have different quantities. Therefore, we can try to calculate potential energies corresponding to all possible sign factors, and those minimizing the potential energy will be the correct solutions of sign factors. For discrete elastic bodies, the potential energy is calculated by the following formula [22]:

$$\prod_p (\eta_r^B, \eta_r^C) = \frac{1}{2}\boldsymbol{u}(\eta_r^B, \eta_r^C)^{\mathrm{T}}\boldsymbol{K}\boldsymbol{u}(\eta_r^B, \eta_r^C) - \boldsymbol{u}(\eta_r^B, \eta_r^C)^{\mathrm{T}}\boldsymbol{F} \tag{5}$$

where $\prod_p (\eta_r^B, \eta_r^C)$ is the potential energy, which is a function with respect to η_r^B and η_r^C. $\boldsymbol{K}$ is the stiffness matrix of the entire structure that is unknown. Substituting Eq. (4) into Eq. (5) and considering the fact that the flexibility matrix is the inverse of the stiffness matrix, Eq. (6) is achieved:

$$\prod_p (\eta_r^B, \eta_r^C) = -\frac{1}{2}\boldsymbol{F}^{\mathrm{T}}\boldsymbol{f}(\eta_r^B, \eta_r^C)\boldsymbol{F} \tag{6}$$

Eq. (7) is derived by substituting Eq. (3) into Eq. (6):

$$\prod_p (\eta_r^B, \eta_r^C) = -\frac{1}{2}\boldsymbol{F}^{\mathrm{T}}\left[\sum_{r=1}^{m}\left(\frac{\boldsymbol{\phi_r}(\boldsymbol{\phi_r})^{\mathrm{T}} Q_r}{-\lambda_r} + \frac{\boldsymbol{\phi_r^*}(\boldsymbol{\phi_r^*})^{\mathrm{T}} Q_r^*}{-\lambda_r^*}\right)\right]\boldsymbol{F} \tag{7}$$

Considering civil engineering structures are mostly light damping structures and the identified mode shapes are generally real values, i.e. $\boldsymbol{\phi_r^*} = \boldsymbol{\phi_r}$, Eq. (7) is simplified as follows:

$$\prod_p (\eta_r^B, \eta_r^C) = \frac{1}{2}\sum_{r=1}^{m}\left[(\boldsymbol{F}^{\mathrm{T}}\boldsymbol{\phi_r})^2\left(\frac{Q_r}{\lambda_r} + \frac{Q_r^*}{\lambda_r^*}\right)\right] \tag{8}$$

The load vector $\boldsymbol{F}$ applied on the entire structure can be rewritten as:

$$\boldsymbol{F} = \begin{bmatrix} \boldsymbol{F^A} \\ \boldsymbol{F^B} \\ \boldsymbol{F^C} \end{bmatrix} \tag{9}$$

where $\boldsymbol{F^A}$, $\boldsymbol{F^B}$ and $\boldsymbol{F^C}$ are the load vectors applying on Sub A, Sub B and Sub C respectively. Substituting Eqs. (2) and (9) into Eq. (8), it is derived that:

$$\prod_p (\eta_r^B, \eta_r^C) = \frac{1}{2}\sum_{r=1}^{m}\left\{\left[(\boldsymbol{F^A})^{\mathrm{T}}\boldsymbol{\phi_r^A} + (\boldsymbol{F^B})^{\mathrm{T}}\boldsymbol{\phi_r^B}\sqrt{\frac{Q_r^B}{Q_r^A}}\eta_r^B + (\boldsymbol{F^C})^{\mathrm{T}}\boldsymbol{\phi_r^C}\sqrt{\frac{Q_r^C}{Q_r^A}}\eta_r^C\right]^2\left(\frac{Q_r}{\lambda_r} + \frac{Q_r^*}{\lambda_r^*}\right)\right\} \tag{10}$$

It is seen that only the sign factors η_r^B and η_r^C equating 1 or -1 are unknown. Trying all possible values of η_r^B and η_r^C for the potential energy calculation through Eq. (10), those minimizing the potential energy will be the solutions of sign factors. This process is illustrated in step 4 of Fig. 5. After η_r^B and η_r^C are solved, the mode shapes of the entire structure are integrated through Eq. (2), and the entire flexibility matrix, illustrated in step 5 of Fig. 5, is identified by Eq. (3).

According to the presentation above, the overall framework and steps to process signals of the developed methodology can be illustrated as follows:

4. Application to a three span simply-supported steel stringer bridge

4.1. Impact test of the bridge

The studied bridge (Fig. 6(a)) comprised of three spans with overall span 48.0 m [23]. Each span harbors a RC deck supported by seven simply-supported I-shape beams spaced at approximately 2.18 m, which are made of rolled steel. Only the south side of the first span was selected as the test area that was closed to traffic during testing (Fig. 6(b)). A total of 24 PCB 393A-03 accelerometers were placed on the bridge deck directly above the bridge girders to measure vertical vibration in the closed traffic lanes and along the opposite sidewalk.

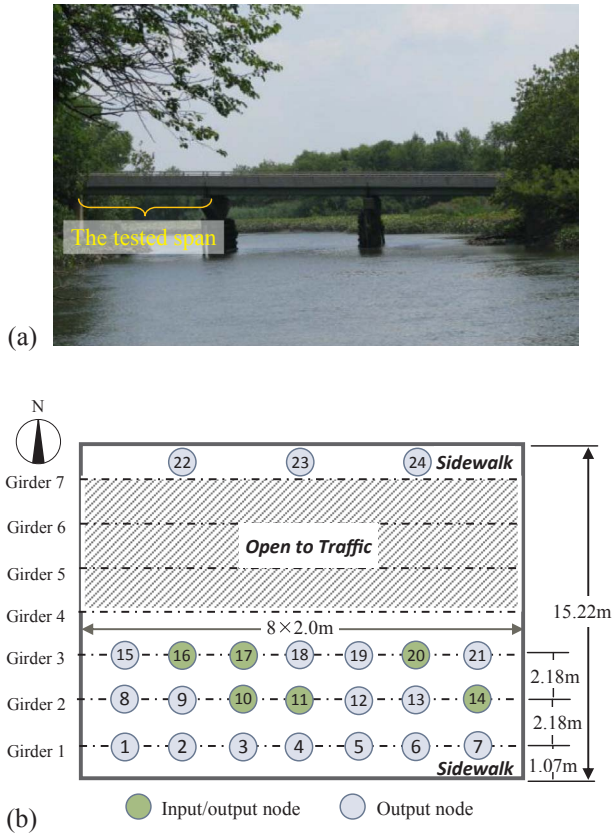

Fig. 6. (a) Photograph of the bridge; (b) Layout of measuring nodes in the tested span.

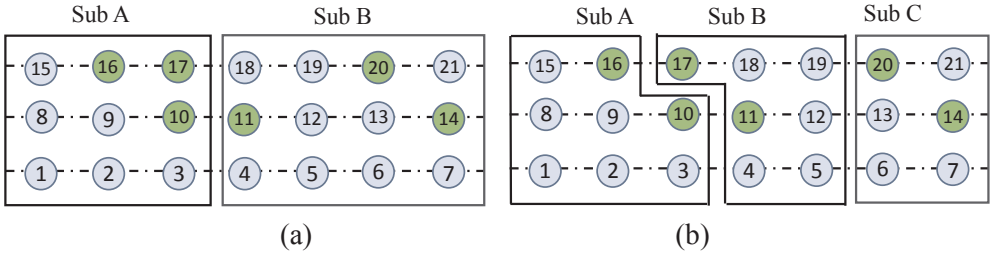

Fig. 7. Substructure division: (a) Scheme 1; (b) Scheme 2.

The sensors on the opposite sidewalk were used to assist in identifying torsional modes. A rebound controlled drop hammer which was capable of applying 110 kN impact force was used to impact the test area [23]. Six locations were used as input points including node 10, 11, 14, 16, 17 and 20. The sampling frequency was configured as 3200 Hz in both acceleration and impacting force. Two schemes for dividing the whole tested area as shown in Fig. 7 for mobile impact testing are studied.

4.2. Basic modal parameter identification

Mobile impact test in Scheme 1 (Fig. 7(a)) is first studied to demonstrate the proposed method. The dimensions of FRFs estimated from two substructures are denoted by $\boldsymbol{H}^{\boldsymbol{AA}}(\omega) \in \mathbb{C}^{9\times3\times32768}$ and $\boldsymbol{H}^{\boldsymbol{BB}}(\omega) \in \mathbb{C}^{12\times3\times32768}$ respectively. The singular curves of two substructures are shown in Fig. 8(b) and (c), and the identified frequencies and damping ratios of the two substructures for the first six modes using CMIF method [15] are listed in Table 1. The results identified from conventional impact test of the whole structure are also provided for comparison in Fig. 8(a) and Table 1. It is seen that those results agree well to each other.

Other basic modal parameters of two substructures are also identified, which can be used to generate the modal parameters of the entire structure. They are denoted by $\{Q_r^A, \boldsymbol{\phi}_r^{\boldsymbol{A}}, \boldsymbol{L}_r^{\boldsymbol{A}}\}$, $\{Q_r^B, \boldsymbol{\phi}_r^{\boldsymbol{B}}, \boldsymbol{L}_r^{\boldsymbol{B}}\}$ for two substructures and $\{Q_r, \boldsymbol{\phi}_r, \boldsymbol{L}_r\}(r = 1,2,...,6)$ for the entire structure, in which $\boldsymbol{\phi}_r^{\boldsymbol{A}} \in \mathbb{R}^{9\times6}$, $\boldsymbol{L}_r^{\boldsymbol{A}} \in \mathbb{C}^{3\times6}$, $\boldsymbol{\phi}_r^{\boldsymbol{B}} \in \mathbb{R}^{12\times6}$, $\boldsymbol{L}_r^{\boldsymbol{B}} \in \mathbb{C}^{3\times6}$, $\boldsymbol{\phi}_r \in \mathbb{R}^{21\times6}$ and $\boldsymbol{L}_r \in \mathbb{C}^{6\times6}$.

4.3. Magnitude scaling of substructures' mode shapes

Since the identified mode shapes of Sub A and Sub B are not at the same scaling level, i.e. $Q_r^A \neq Q_r^B$, magnitude adjustments are needed when integrating them as the global mode shapes. Because the number of output nodes in Sub B is larger than that in Sub A, Sub B is chosen as the master segment. A total six magnitude adjustment factors of Sub A are calculated by Eq. (1) using identified Q_r^A and Q_r^B. The results are listed in Table 2.

It should be noted that the signs of those magnitude adjustment factors are still unknown. Taking the second mode as an example and assuming that its sign factor equals to 1, Fig. 9 illustrates the process of mode shape scaling. The global mode shape, identified with the traditional impact test of the entire structure and marked with the black solid line in the figure, is also provided for comparison. It is seen that the scaled mode shape of Sub A matches well with the global mode shape at the corresponding nodes when assuming $\eta_2^A = 1$. The next work describes how to determine the sign factors via the proposed method.

4.4. Sign factor determination by PMPE

For the first six modes, there are six sign factors, $\eta_r^A (r = 1,...,6)$, that need to be determined, which equals 1 or -1. PMPE-based approach described in Section 3.2 is performed to determine sign factors. If one tries all possible combinations of sign factors, for instance, $\eta_1^A = 1, \eta_2^A = -1, \eta_3^A = 1, \eta_4^A = -1, \eta_5^A = 1, \eta_6^A = -1$ is a possible combination, there are $2^6 = 64$ cases considering any combinations of either 1 or -1 among six sign factors. Each node is applied a 5 kN load to calculate displacement and potential energy through Eqs. (4) and (10) for all 64 possible cases respectively, but among which, theoretically, only the case having the minimum potential energy is the correct one according to PMPE. Thus the authors firstly enumerate the 64 quantities

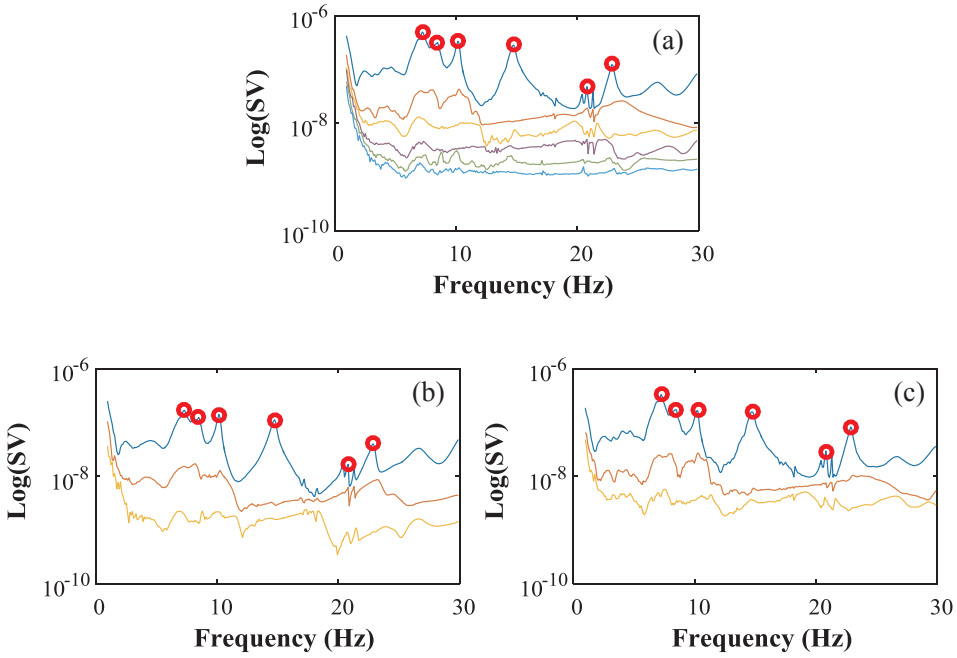

Fig. 8. Singular value of: (a) Entire structure; (b) Sub A; (c) Sub B.

Table 1
Identified frequency and damping ratio (Scheme 1).

Mode No.	Entire structure		Sub A		Sub B	
	Freq. (Hz)	Damp. (%)	Freq. (Hz)	Damp. (%)	Freq. (Hz)	Damp. (%)
1	7.16	6.53	7.25	7.91	7.13	5.71
2	8.26	5.24	8.25	4.58	8.22	6.20
3	10.14	1.38	10.12	1.38	10.14	1.32
4	14.71	1.76	14.68	1.65	14.70	1.86
5	20.76	0.56	20.57	0.31	20.80	0.66
6	22.85	0.97	22.78	1.08	22.82	0.93

Table 2
Magnitude adjustment factor and MAC value (Scheme 1).

Mode No.	$\sqrt{Q_r^A/Q_r^B}$	MAC
1	0.67	0.9996
2	0.64	0.9992
3	0.65	0.9994
4	0.63	0.9999
5	0.84	0.9856
6	0.72	0.9962

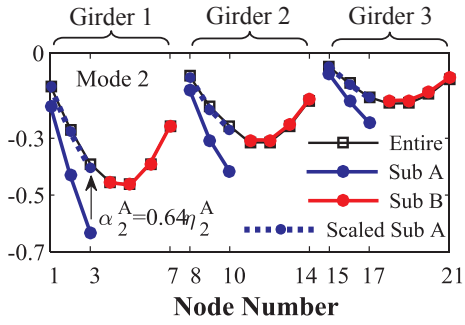

Fig. 9. Typical mode shapes scaling (Scheme 1).

of all possible potential energies in ascending order, and then the sequence can be depicted with the gray curve shown in Fig. 10(a), in which the scenario of the minimum potential energy (rank 1, −39.93 J) is highlighted with a blue pentagram.

In order to further study the influence of mode order on potential energy, the potential energy for each case is calculated by sequentially setting up mode number m = 1,2,...,6 in Eq. (10). Fig. 10(b) depicts the relation between the potential energy of each case and order m. It can be seen that as order increases to six, potential energy for each case gradually converges to a stable level, whereas only PE of rank 1 has the minimal potential energy at the sixth order. This is because modal flexibility generally rapidly converges to the structural flexibility with the increasing of mode order [20,21].

Deflections predicted through Eq. (4) in typical cases (ranked 1, 16, 32, 48, 64 corresponding to PE) when each node is applied a 5 kN load are plotted in Fig. 11 for comparison, and the deflection predicted by

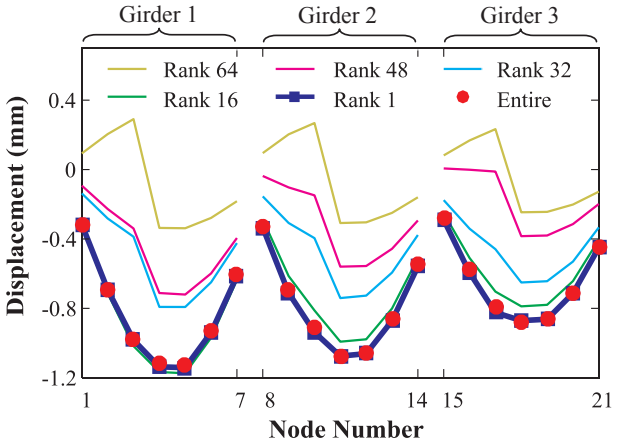

Fig. 11. Deflections comparison in typical cases (Scheme 1).

the traditional impact test method marked with “Entire” is also plotted to be the reference. It is seen that the minimum PE-based deflection agrees well with the referenced deflection, while these deflections corresponding to non-minimum quantities of PE do not more or less match with the referenced deflection, which demonstrates the effectiveness of PMPE-based approach for displacement prediction.

In the authors’ computation, all sign factors extracted from PE of rank 1 for scheme 1 are equal to 1. Whether those sign factors are correct or not should be checked by comparing the integrated mode shapes with the referenced global mode shapes identified from traditional impact test method. For the sake of brevity, the integrated mode shapes and the global mode shapes are depicted in Fig. 12 with three dimensional maps. It can be seen that their well proximity certifies the correctness of sign factors extracted from PE of rank 1 and the high accuracy of integrated mode shapes. In addition, the values of modal assurance criterion (MAC) closing to 1 listed in Table 2 further quantitatively demonstrate that the mobile impact test with reference-free measurement can achieve the equivalent results as the conventional impact test method which requires to measure all inputs and outputs nodes.

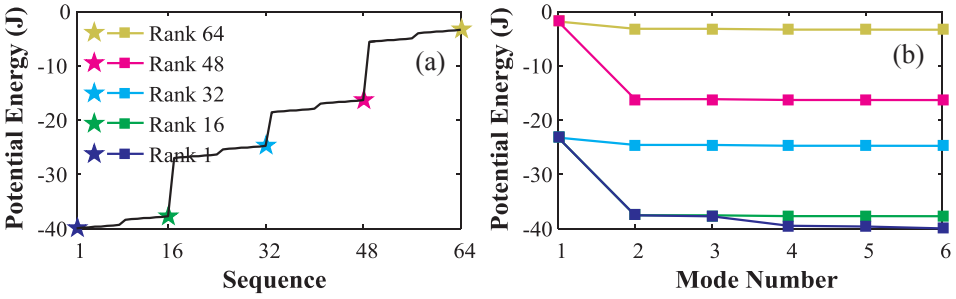

Fig. 10. PE curves corresponding to: (a) Sequence; (b) Mode number (Scheme 1).

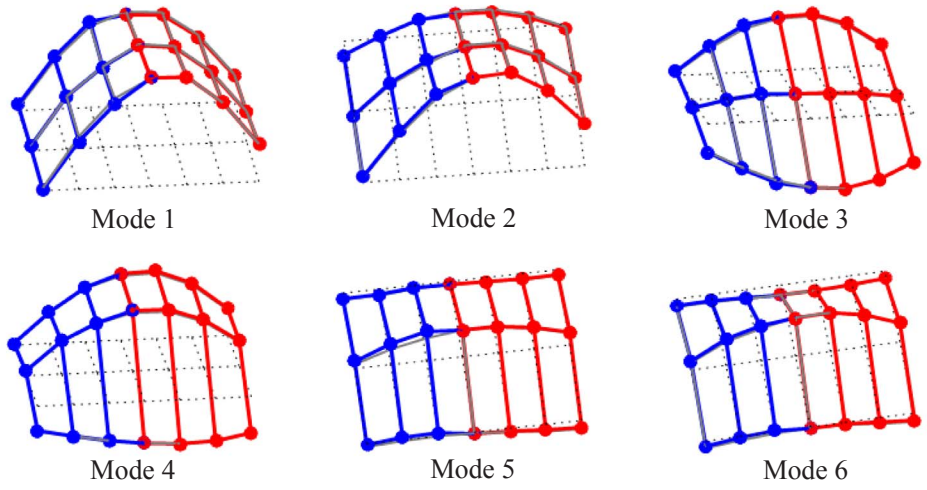

Fig. 12. 3-D map of the six integrated mode shapes (Scheme 1).

4.5. Full flexibility matrix identification

The full flexibility matrix of the bridge, denoted by $\boldsymbol{f} \in \mathbb{R}^{21\times21}$, can be calculated through Eq. (3) using the six integrated mode shapes, the six system poles and modal participation factors of Sub B. Fig. 13 clearly shows its 3-D surface map and as can be seen from it, the maximum flexibility coefficient is $f_{55} = 2.1 \times 10^{-8}$ m/N, which extremely closes to the coefficient obtained from the traditional impact test method.

To check with whether the modal order, six modes in Scheme 1, will influence displacement prediction or not, meanwhile to study effects of mode number truncation, Fig. 14 illustrates the predicted deflections when each node is applied a 5 kN load, in which the curve denoted by "4 modes" in Fig. 14 refers to the modal parameters of the first fours modes contributing to the flexibility matrix in Eq. (3). It can be seen that the first four modes already insure the accuracy of displacement prediction for the real bridge and thus six modes of modal parameters are sufficient for flexibility identification.

4.6. Results of Scheme 2

Scheme 2 that has complex substructures division is adopted to further validate the feasibility of the reference-free flexibility integration method. In Scheme 2, Sub B is chosen as the master substructure and mode shapes of Sub A and Sub C should be adjusted to be consistent with that of Sub B. The amount for sign factors, $\eta_r^A, \eta_r^C (r = 1,...,6)$, falls

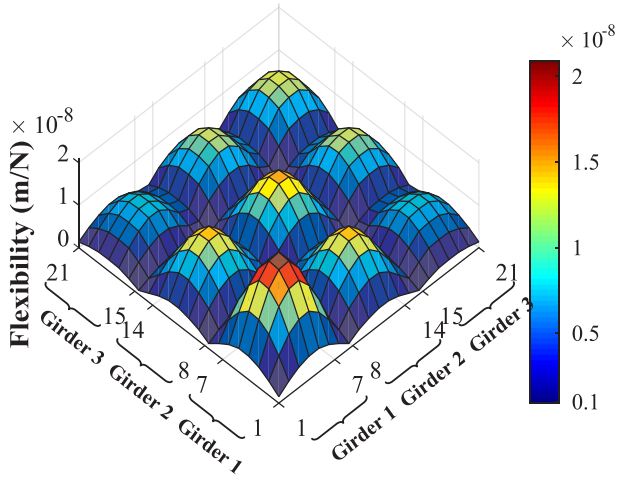

Fig. 13. 3-D map of the identified full flexibility matrix (Scheme 1).

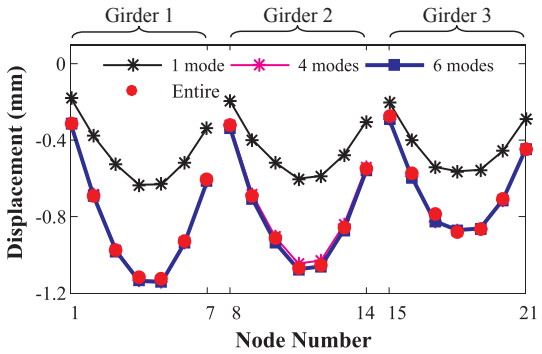

Fig. 14. Deflections prediction when each node is applied a 5 kN load (Scheme 1).

into $2^{6(3-1)} = 4096$ cases considering any combinations of either 1 or −1 among six modes of two sign factors. Fig. 15(a) illustrates the sorted PE for all cases in ascending order when each node is applied a 4.445 kN load, in which the calculated minimum PE (rank 1, −32.36 J) is highlighted with a blue pentagram.

Similarly to the situation presented in Fig. 10(b), the effect of modal number truncation on potential energy in each case is depicted in Fig. 15(b). It can be seen that as order increases to six, potential energy for each case gradually converges to a stable level, whereas only PE of rank 1 has the minimal PE at the sixth mode.

For the sake of brevity, the sign factors extracted from PE of rank 1 for scheme 2 have not been provided here, and the magnitude adjustment factors calculated from Eq. (1) and MAC values calculated from the integrated mode shapes and the referenced mode shapes are listed in Table 3. It is evident that the high MAC values closing to 1 validate the correctness of sign factors extracted from PE of rank 1 and the high accuracy of the integrated mode shapes in Scheme 2.

The integrated full flexibility matrix can be briefly used to simulate static test on the bridge and hence the deflections induced by truck loads can be predicted. Assuming a truck with total weight of 300 kN parks on the bridge and its four wheels just press on node 10, 12, 17, 19 respectively, each wheel will apply 75 kN to the interacted nodes. Fig. 16 illustrates the deflections predicted by the integrated full flexibility matrix in Scheme 2. The error due to mode number truncation is studied. It can be seen that using the first four modes are able to sufficiently capture the flexibility characteristics of the real bridge despite only the first six modes of modal parameters have been obtained.

In practice, adopting different master substructure will influence the results of full flexibility matrix integrated. Generally, a reasonable substructure with effective partition and stable modal parameters identified should be adopted as the master segment. Furthermore, for

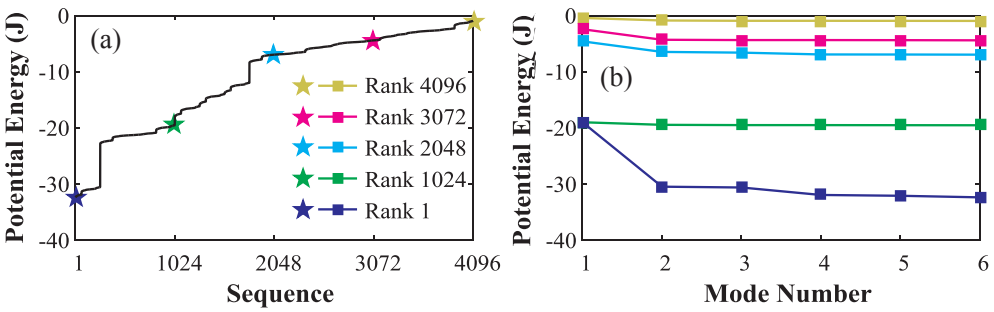

Fig. 15. PE curves corresponding to: (a) Sequence; (b) Mode number (Scheme 2).

Table 3
Magnitude adjustment factor and MAC value (Scheme 2).

Mode No.	$\sqrt{Q_r^A/Q_r^B}$	$\sqrt{Q_r^C/Q_r^B}$	MAC
1	0.75	0.66	0.9982
2	0.77	0.78	0.9946
3	0.53	0.64	0.9992
4	0.58	0.67	0.9998
5	1.05	1.03	0.9452
6	0.86	0.76	0.9950

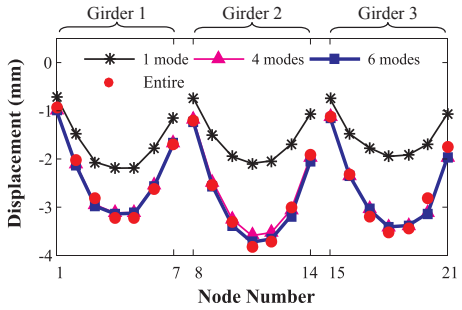

Fig. 16. Deflections prediction for a truck of 300 kN (Scheme 2).

complex substructures divisions, some modes of a certain substructure may be lost if the node being impacted just place on one of nodes of vibration. But this question can be overcome by performing multiple reference impact testing (MRIT), i.e., impacting different nodes (at least two nodes) in each substructure.

5. Conclusions

This paper presents a rapid mobile impact test method for structural flexibility identification. The method makes up for the shortcomings of traditional one-off shock and vibration testing method, and truly realizes the overall identification of structural parameters. The key technology is how to integrate the observed vibration data of all substructures to get the entire structural identification results consistent with the test results of traditional impact test method. The conclusions are as follows:

(1) A pure reference-free mobile impact test approach has been proposed. It tests each subdivided segment in turn and the recorded data are used to identify each segment's modal parameters. The adjusting factors and PMPE are utilized to integrate isolated mode shapes of each mode into the global mode shapes of the entire structure and get the full flexibility matrix.
(2) Comparing to the conventional impact test method which measures all inputs and outputs signals, the proposed method can obtain the same results but needs less instrumentation and test time as well as cost, therefore it has great potentialities in rapid testing and monitoring of short/middle span bridges.
(3) Application of the proposed approach to an actual bridge successfully verifies its feasibility and efficiency for identifying the full flexibility matrix. Furthermore, the experimental study approves that the number and formation of substructures can be divided flexibly.
(4) Higher modes have little influence on the potential energy and the minimum potential energy cannot guarantee the correctness of the automatic determination of the sign factors in higher modes. The way to identify higher modes information will be studied in the future, even though the identified modes have met the requirement of accuracy as shown in this article.

Acknowledgments

This work was sponsored by the Chinese National Science Foundation (Grant Nos. 51578139, 51608110). Dr. Jeffrey Weidner, Dr. John Prader, Dr. Nathern Dubbs, Dr. Matthew Yarnold, Mr. John DeVitis and Miss Adrienne Deal, are acknowledged for their contribution to the field test of the studied bridge.

Appendix A. Supplementary material

Supplementary data associated with this article can be found, in the online version, at http://dx.doi.org/10.1016/j.engstruct.2017.12.020.

References

[1] Catbas FN, Tracy KC, Aktan AE. Structural identification of constructed facilities: approaches, methods and technologies for effective practice of St-Id. ASCE SEI Committee on Structural Identification of Constructed Systems; 2012.
[2] Kim S, Pakzad S, Culler D, Demmel J, Fenves G, Glaser S, et al. Health monitoring of civil infrastructures using wireless sensor network. In: Proceedings of the 6th international symposium on information processing in sensor networks. Cambridge, Massachusetts, USA; 2007.
[3] Marulanda J, Caicedo JM, Thomson P. Modal identification using mobile sensors under ambient excitation. ASCE J Comput Civ Eng 2016;04016051.
[4] Xia Q, Cheng YY, Zhang J, Zhu FQ. In-service condition assessment of a long-span suspension bridge using temperature-induced strain data. ASCE J Bridge Eng 2017;22(3).
[5] Zimmerman AT, Shiraishi M, Swartz RA, Lynch JP. Automated modal parameter estimation by parallel processing within wireless monitoring systems. ASCE J Infrastruc Syst 2008;14(1):102–13.
[6] Sim SH, Spencer BF, Zhang M, Xie H. Automated decentralized modal analysis using smart sensors. Struct Control Health Monit 2010;17:872–94.
[7] Sadhu A, Hazra B, Narasimhan S, Pandey MD. Decentralized modal identification using sparse blind source separation. Smart Mater Struct 2011;20:125009.
[8] Lynch JP. An overview of wireless structural health monitoring for civil structures. Roy. Soc., London 2007;365:345–72.
[9] Li ZH, Au FTK. Damage detection of bridges using response of vehicle considering road surface roughness. Int J Struct Stab Dyn 2015;15(3):1–28.
[10] Adewuyi AP, Wu ZS. Modal macro-strain flexibility methods for damage localization in flexural structures using long-gage FBG sensors. Struct Control Health Monit 2011;18(3):341–60.
[11] Brownjohn JMW, Magalhaes F, Caetano E, Cunha A. Ambient vibration re-testing and operational modal analysis of the Humber Bridge. Eng Struct 2010;32(8):2003–18.
[12] Brown DL, Witter MC. Review of recent developments in multiple-reference impact testing. Sound Vib 2011;45(1):8–17.
[13] Zhou Y, Prader J, Weidner J, Dubbs N, Moon F, Aktan AE. Structural identification of a deteriorated reinforced concrete bridge. ASCE J Bridge Eng 2012;17:774–87.
[14] Zhang J, Guo SL, Chen X. Theory of un-scaled flexibility identification from output-

only data. Mech Syst Sig Process 2014;48(1–2):232–46.
[15] Catbas FN, Brown DL, Aktan AE. Use of modal flexibility for damage detection and condition assessment: case studies and demonstrations on large structures. ASCE J Struct Eng 2006;132(11):1699–712.
[16] Yang YB, Lin CW. Vehicle-bridge interaction dynamics and potential applications. J Sound Vib 2005;284(1–2):205–26.
[17] Xiang ZH, Dai XW, Zhang Y, Lu QH. The tap-scan method for damage detection of bridge structures. Interact Multiscale Mech 2010;3:173–91.
[18] Guo W, Soibelman L, Garrett J. Visual pattern recognition supporting defect reporting and condition assessment of wastewater collection systems. ASCE J Comput Civ Eng 2009;23(3):160–9.
[19] De Vitis J, Masceri D, Aktan AE, Moon F. Rapid structural identification methods for highway bridges: towards a greater understanding of large populations. Proceedings of the 11th international conference on structural safety & reliability. NY, USA: Columbia University; 2013.
[20] Zhang J, Moon F. A new impact testing method for efficient structural flexibility identification. Smart Mater Sruct 2012;21(21):55–71.
[21] Zhang J, Guo SL, Zhang QQ. Mobile impact testing for structural flexibility identification with only a single reference. Comput-Aided Civ Infrastruc Eng 2015;30(9):703–14.
[22] Clough R, Penzien J. Dynamics of structures. McGraw-Hill Book Co.; 1975.
[23] Prader JB. Rapid impact modal testing for bridge flexibility: towards objective evaluation of infrastructures [Ph.D. Dissertation]. Philadelphia, USA: Drexel University; 2012.